2-phenylbenzoxazole derivatives as solid-state fluorescence emitters: Influence of steric hindrance and hydrogen bonding on the optical properties

Emma Bremond, Nadine Leygue, Nathalie Merceron-Saffon, Suzanne Fery-Forgues

2-phenylbenzoxazole derivatives as solid-state fluorescence emitters: Influence of steric hindrance and hydrogen bonding on the optical properties

Emma Bremond [a], Nadine Leygue [a], Nathalie Saffon-Merceron [b] and Suzanne Fery-Forgues [a]*

[a] *SPCMIB, UMR 5068, CNRS-Université de Toulouse III Paul Sabatier, 118 route de Narbonne, Toulouse, 31062, France*
[b] *Service commun RX, Institut de Chimie de Toulouse, ICT- FR2599, Université de Toulouse III Paul Sabatier, 31062 Toulouse cedex 9, France.*
** Corresponding author. E-mail address: sff@chimie.ups-tlse.fr (S. Fery-Forgues)*

ABSTRACT
Six new 2-phenylbenzoxazole (PBO) derivatives, bearing either a methoxy or hydroxyl group at position 5, were prepared via an efficient one-step synthesis that allowed both analogues to be obtained in equal proportions. These PBO derivatives also differed by the presence or absence of an alkyl substituent at the *para*-position of the phenyl group. In organic solutions, all six compounds were strongly fluorescent in the near-UV range. In the solid state, the 5-methoxy derivatives emitted bright light, ranging from violet to deep blue according to the substitution of the phenyl group. The presence of a bulky *tert*-butyl group indeed resulted in the separation of molecules, but also led to a deviation from molecular planarity. Remarkably, the introduction of a methyl group had a far more beneficial effect on the optical properties. With regard to the hydroxyl derivatives, none of them was photoluminescent, probably due to strong intermolecular hydrogen bonding in the crystals. The 50:50 mixtures of methoxy and hydroxyl analogues showed acceptable emission properties in the solid state. The substitution pattern also influenced the crystal habit of the pure compounds and the crystallinity of the mixtures. These cheap molecules could be adapted to suit a variety of applications in the field of photoluminescent materials.

Keywords
2-Phenylbenzoxazole
Solid-state emission
Fluorescence
Photoluminescence
Crystal structure
Hydrogen bonding

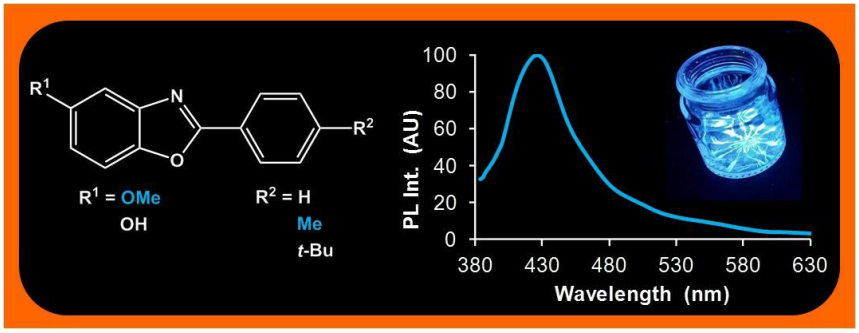

1. Introduction

Organic dyes that emit efficiently in the blue in the solid state are currently scarce and much sought after, especially for applications in the field of optoelectronics [1, 2]. Their development is hampered by the difficulty to predict their photoluminescence properties, which closely depend on the molecular arrangement [3, 4]. In particular, fluorescence is generally quenched by aggregation, due to

π-π stacking of aromatic moieties. One of the strategies [5] used to circumvent this problem is selecting one molecule with appropriate photoluminescence properties, and studying in a systematic way the influence of small chemical modifications upon the molecular arrangement and optical properties.

During the last decade, this strategy has been implemented in our group starting from 2-phenylbenzoxazole (PBO), a low-molecular weight compound that displays outstanding chemical, thermal and photochemical stability. As recently reviewed, many dyes of this family show excellent fluorescence properties in the solid state, with emission ranging from deep-blue to orange [6]. Some of them have been used as blue emitters in OLEDs [7, 8]. Most of the time, chemical modifications are introduced in the *para* position of the phenyl group for synthesis conveniences, and the influence of other substitution patterns on the solid-state properties has not been explored. In the present work, a methoxy group has been introduced in the 5-position of PBO with the aim to shift the solid-sate emission spectrum from UV to the visible range owing to the weak electron-donating character of this group. Some of our previous works have also shown that the strong structuring effect of the methoxy group in the crystalline state is associated to highly emissive materials [9, 10]. A comparison was made with hydroxyl analogues to highlight the effect of possible hydrogen bonds. Besides, the effect of steric hindrance was also studied by comparing molecules whose phenyl group was either unsubstituted, or substituted by a methyl or a *tert*-butyl group. It was expected that the latter group, known to influence the crystal packing mode of closely related PBOs [11], would separate molecules and favour light emission in the solid state [12-15]. Therefore, compounds **1** to **6** (Fig. 1) were prepared. Their spectroscopic properties were investigated in solution and in the solid state, and compared with the previously studied compounds **7-9** that do not bear oxygenated function at position 4 [11]. A relationship was made between the solid-state properties of the new compounds and their crystallographic characteristics, allowing the effect of the various substituents to be better understood. The influence of the substituents upon the crystal shape was also briefly regarded.

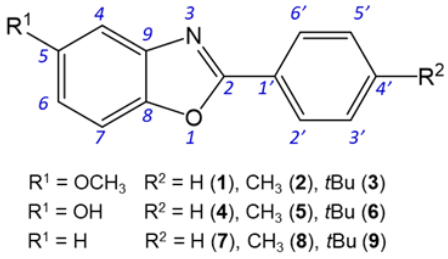

Fig. 1. Chemical structure of the 2-phenylbenzoxazole derivatives.

2. Materials and methods

2.1. Materials and characterization

Absolute ethanol Chromasol quality (Sigma-Aldrich), as well as analytical grade solvents from SDS were used as received. 2-Amino-4-methoxyphenol and the various acyl chlorides were purchased from Aldrich. Reactions were monitored by analytical TLC using silica gel on aluminium sheets (Kieselgel 60 F254, Merck) under UV light (254 nm). Chromatographic purifications were made using silica gel (60-200 μm, porosity 60 Å) purchased from Merck.

General synthesis procedure. To a solution of 2-amino-4-methoxyphenol (0.2520 g, 1.81 mmol) in 1 mL *N*-methylpyrrolidinone (NMP), acid chloride in stoichiometric proportion was added dropwise under argon and left to stand under stirring at 0 °C for 1h. After addition of pyridine (0.23 mL), the mixture was brought to reflux of NMP (bp: 202 °C) for 2h. After cooling to room temperature, the crude was portioned between water (10 mL) and dichloromethane. The organic layer was separated and the aqueous layer was extracted twice with dichloromethane. The combined organic layers were dried with $MgSO_4$, the solvent was removed and the residue was purified by column chromatography on silica gel, yielding the methoxy and hydroxyl analogues with yields close to 46% for each of them.

2-Phenyl-5-methoxybenzoxazole (**1**)

TLC (SiO_2, petroleum ether/ethyl acetate 80:60) R_f = 0.40. Mp = 78°C. ^{1}H NMR (300 MHz, CD_3OD): δ ppm = 8.22-8.17 (m, 2H, $H_{2'}$ and $H_{6'}$), 7.60-7.56 (m, 3H, $H_{4'}$, $H_{3'}$, $H_{5'}$), 7.54 (dd, J = 9, 0.6 Hz, 1H, H_7), 7.22 (dd, J = 2.6, 0.6 Hz, 1H, H_4), 7.00 (dd, J = 9.0, 2.6 Hz, 1H, H_6), 3.86 (s, 3H, CH_3). NMR ^{13}C (75 MHz, CD_3OD): δ ppm = 165.3 (Cq, C_2), 159.3 (Cq, C_5), 146.6 (Cq, C_9), 143.6 (Cq, C_8), 133.0 (CH, $C_{4'}$), 130.2 (CH, $C_{3'}$ and $C_{5'}$), 128.4 (CH, $C_{2'}$ and $C_{6'}$), 128.1 (Cq, $C_{1'}$), 115.2 (CH, C_6), 112.0 (CH, C_7), 103.5 (CH, C_4), 56.4 (CH_3, OCH_3). MS (ESI^+): *m/z* 226.0 ($[M+H]^+$, 100%), HRMS (ESI^+): *m/z* calcd for $C_{14}H_{12}NO_2$ $[M+H]^+$ 226.0868; found 226.0872. IR: 1622 cm^{-1} ($\nu_{C=N}$), 1553 cm^{-1} ($\nu_{-N=C-O-}$), 1426-1480 cm^{-1} ($\nu_{C=C}$), 1111 cm^{-1} (ν_{C-O}).

2-Toluyl-5-methoxybenzoxazole (**2**)

TLC (SiO_2, petroleum ether/ethyl acetate 80:20) R_f = 0.50. Mp = 116°C. ^{1}H NMR (300 MHz, CD_3OD): δ ppm = 8.08-8.04 (m, 2H, $H_{2'}$ and $H_{6'}$), 7.52 (dd, J = 8.9, 0.7 Hz, 1H, H_7), 7.39-7.35 (m, 2H, $H_{3'}$, $H_{5'}$), 7,20 (dd, J = 2.6, 0.8 Hz, 1H, H_4), 6.97 (dd, J =8.9, 2.6 Hz, 1H, H_6), 3.86 (s, 3H, OCH_3), 2.43 (s, 3H, CH_3). ^{13}C NMR (75 MHz, CD_3OD): δ ppm = 165.5 (Cq, C_2), 159.2 (Cq, C_5), 146.5 (Cq, C_9), 143.9 (Cq, $C_{4'}$), 143.6 (Cq, C_8), 130.8 (CH, $C_{3'}$ and $C_{5'}$), 128.4 (CH, $C_{2'}$ and $C_{6'}$), 125.3 (Cq, $C_{1'}$), 114.8 (CH, C_6), 111.9 (CH, C_7), 103.3 (CH, C_4), 56.4 (CH_3, OCH_3), 21.6 (CH_3). MS (ESI^+): *m/z* 240.1 ($[M+H]^+$, 100%), HRMS (ESI^+): *m/z* calcd for $C_{15}H_{14}NO_2$ $[M+H]^+$ 240.1025; found 240.1028. IR: 1610 cm^{-1} ($\nu_{C=N}$), 1556 cm^{-1} ($\nu_{-N=C-O-}$), 1408-1479 cm^{-1} ($\nu_{C=C}$), 1106 cm^{-1} (ν_{C-O}).

2-(4'-*tert*-Butylphenyl)-5-methoxybenzoxazole (**3**)

TLC (SiO_2, petroleum ether/ethyl acetate 90:10) R_f = 0.45. Mp = 94°C. ^{1}H NMR (300 MHz, CD_3OD): δ ppm = 8.13-8.09 (m, 2H, $H_{2'}$ and $H_{6'}$), 7.63-7.58 (m, 2H, $H_{3'}$ and $H_{5'}$), 7.52 (dd, J = 8.9, 0.6 Hz, 1H, H_7), 7.21 (dd, J = 2,7, 1H, H_4), 6.98 (dd, J = 8.9, 2.6 Hz, 1H, H_6), 3.86 (s, 3H, CH_3), 1.37 (s, 9H, CH_3). ^{13}C NMR (75 MHz, CD_3OD): δ ppm = 165.5 (Cq, C_2), 159.2 (Cq, C_5), 156.8 (Cq, $C_{4'}$), 146.5 (Cq, C_9), 143.6 (Cq, C_8), 128.3 (CH, $C_{3'}$ and $C_{5'}$), 127.2 (CH, $C_{2'}$ and $C_{6'}$), 125.2 (Cq, $C_{1'}$), 114.9 (CH, C_6), 111.9 (CH, C_7), 103.4 (CH, C_4), 56.4 (CH_3, OCH_3), 36.0 (Cq, *t*Bu), 31.5 (CH_3, *t*Bu). MS (ESI^+): *m/z* 282.1 ($[M+H]^+$, 100%), HRMS (ESI^+): *m/z* calcd for $C_{18}H_{20}NO_2$ $[M+H]^+$ 282.1494; found 282.1491. IR : 1611 cm^{-1} ($\nu_{C=N}$), 1553 cm^{-1} ($\nu_{-N=C-O-}$), 1412-1482 cm^{-1} ($\nu_{C=C}$), 1115 cm^{-1} (ν_{C-O}).

2-Phenyl-5-hydroxybenzoxazole (**4**)

TLC (SiO_2, dichloromethane/methanol 97:3) R_f = 0.30. Mp = 176°C. ^{1}H NMR (300 MHz, CD_3OD): δ ppm = 8.22-8.16 (m, 2H, $H_{2'}$ and $H_{6'}$), 7.60-7.54 (m, 3H, $H_{3'}$, $H_{4'}$, $H_{5'}$), 7.47 (dd, J = 8.8, 0.8 Hz, 1H, H_7), 7.09 (dd, J =2.5, 0.8 Hz, 1H, H_4), 6.88 (dd, J = 8.9, 2.4 Hz, 1H, H_6). ^{13}C NMR (75 MHz, CD_3OD) :

δ ppm = 165.1 (Cq, C_2), 156.6 (Cq, C_5), 146.0 (Cq, C_9), 143.6 (Cq, C_8), 132.9 (CH, $C_{4'}$), 130.2 (CH, $C_{3'}$, $C_{5'}$), 128.4 (CH, $C_{2'}$, $C_{6'}$), 128.1 (Cq, $C_{1'}$), 115.2 (CH, C_6), 111.8 (CH, C_7), 105.5 (CH, C_4). MS (ESI^+): *m/z* 212.0 ($[M+H]^+$, 100%), HRMS (ESI^+): *m/z* calcd for $C_{13}H_{10}NO_2$ $[M+H]^+$ 212.0712, found 212.0711. IR: 3153 cm^{-1} (ν_{O-H}), 1621 cm^{-1} ($\nu_{C=N}$), 1549 cm^{-1} ($\nu_{-N=C-O-}$), 1390-1472 cm^{-1} ($\nu_{C=C}$).

2-(4'-Toluyl)-5-hydroxybenzoxazole (**5**)

TLC (SiO_2, dichloromethane/methanol 97:3) R_f = 0.40. Mp = 201°C. ^1H NMR (300 MHz, CD_3OD): δ ppm = 8.01-7.97 (m, 2H, $H_{2'}$ and $H_{6'}$), 7.40 (dd, 1H, *J* = 8.8, 0.6 Hz, H_7), 7.31-7.27 (m, 2H, $H_{3'}$ and $H_{5'}$), 7.05 (dd, 1H, *J* = 2.5, 0.5 Hz, H_4), 6.84 (dd, 1H, *J* = 8.8, 2.5 Hz, H_6), 2.38 (s, 3H, CH_3). ^{13}C NMR (75 MHz, CD_3OD): δ ppm = 165.3 (Cq, C_2), 156.4 (Cq, C_5), 145.8 (Cq, C_9), 143.7 (Cq, $C_{4'}$), 143.5 (Cq, C_8), 130.7 (CH, $C_{3'}$ and $C_{5'}$), 128.3 (CH, $C_{2'}$ and $C_{6'}$), 125.2 (Cq, $C_{1'}$), 114.9 (CH, C_6), 111.6 (CH, C_7), 105.3 (CH, C_4), 21.6 (CH_3). MS (ESI^+): *m/z* 226.0 ($[M+H]^+$, 100%), HRMS (ESI^+): *m/z* calcd for $C_{14}H_{12}NO_2$ $[M+H]^+$ 226.0868; found 226.0866. IR: 3192 cm^{-1} (ν_{O-H}), 1613 cm^{-1} ($\nu_{C=N}$), 1552 cm^{-1} ($\nu_{-N=C-O-}$), 1419-1500 cm^{-1} ($\nu_{C=C}$).

2-(4'-*tert*-Butylphenyl)-5-hydroxybenzoxazole (**6**)

TLC (SiO_2, dichloromethane/ethylacetate 90:10) R_f = 0.3. Mp = 224°C. ^1H NMR (300 MHz, CD_3OD): δ ppm = 8.12-8.07 (m, 2H, $H_{2'}$ and $H_{6'}$), 7.62-7.57 (m, 2H, $H_{3'}$ and $H_{5'}$), 7.45 (dd, *J* = 8.8, 0.6 Hz, 1H, H_7), 7.08 (dd, *J* = 2.5, 0.6 Hz, 1H, H_4), 6.86 (dd, *J* = 8.9, 2.4 Hz, 1H, H_6), 1.37 (s, 9H, CH_3). ^{13}C NMR (75 MHz, CD_3OD): δ ppm = 165.3 (Cq, C_2), 156.7 (Cq, $C_{4'}$), 156.5 (Cq, C_5), 145.9 (Cq, C_9), 143.5 (Cq, C_8), 128.3 (CH, $C_{3'}$ and $C_{5'}$), 127.2 (CH, $C_{2'}$ and $C_{6'}$), 125.3 (Cq, $C_{1'}$), 114.9 (CH, C_6), 111.7 (CH, C_7), 105.4 (CH, C_4), 35.9 (Cq, *t*Bu), 31.5 (CH_3, *t*Bu). MS (ESI^+): *m/z* 268.1 ($[M+H]^+$, 100%), HRMS (ESI^+): *m/z* calcd for $C_{17}H_{18}NO_2$ $[M+H]^+$ 268.1338; found 268.1336. IR: 3122 cm^{-1} (ν_{O-H}), 1609 cm^{-1} ($\nu_{C=N}$), 1550 cm^{-1} ($\nu_{-N=C-O-}$), 1363-1480 cm^{-1} ($\nu_{C=C}$).

2.2. Apparatus and methods

The melting points were measured on a Melting Point System MP50 Mettler Toledo apparatus. Chemical characterizations were performed in the relevant services of Institut de Chimie de Toulouse (ICT). The ^1H NMR and ^{13}C NMR spectra were recorded on a Bruker AC300 spectrometer operating at 300 MHz and 75 MHz, respectively. Chemical shifts are reported in ppm, with residual protonated solvents as the internal references. Protons and carbon atoms were numbered according to Fig. 1. Electrospray (ES) mass spectra and High- Resolution Mass Spectra (HRMS) were obtained on a Xevo G2 QTof Waters spectrometer. Infrared spectra were obtained using a Nexus ThermoNicolet FTIR spectrophotometer equipped with a diamond ATR.

Spectroscopic measurements in solution were conducted at 20 °C in a temperature-controlled cell of 1 cm optical pathway. Both UV-visible absorption and fluorescence spectra were recorded with a Xenius SAFAS spectrofluorimeter. All fluorescence spectra were corrected. The relative fluorescence quantum yields (Φ_F) of solutions were determined using the classical formula:

$$\Phi_{Fx} = (A_s \times F_x \times n_x^2 \times \Phi_{Fs})/(A_x \times F_s \times n_s^2) \quad (1)$$

where A is the absorbance at the excitation wavelength, F is the area under the fluorescence curve, and n is the refraction index. Subscripts "s" and "x" refer to the standard and to the sample of unknown quantum yield, respectively. Quinine sulfate in 0.1N $HClO_4$ (Φ_F = 0.59) was taken as the standard [16]. The absorbance of the solutions was equal or below 0.050 at the excitation wavelength. The error on Φ_{Fx} values is estimated to be about 10%. For solid samples, the photoluminescence was analyzed on the same apparatus using a $BaSO_4$ integrating sphere. Solid samples were deposited on a metal support. The excitation source was scanned in order to evaluate the reflected light for the empty sphere (L_a), the samples facing the source light (L_c) and the sample out of the irradiation beam (L_b). The luminescence spectra were recorded with the sample facing the source light (E_c) and out from direct irradiation (E_b). The PM voltage was adapted to the measurement of reflected light and emission spectra, respectively, and proper correction was applied to take into account the voltage difference. The absolute photoluminescence quantum yield values (Φ_{PL}) were calculated by a method based on the one developed by de Mello *et al.* [17] using the formula:

$$\Phi_{PL} = [E_c\text{-}(1\text{-}\alpha)E_b]/L_a\alpha \qquad (2)$$

with $\alpha = 1\text{-}L_c/L_b$. The error on the Φ_{PL} value was estimated to be about 20%.

2.3. Crystallography

Crystal data of **2** were collected at 193(2)K using a Bruker-AXS APEX II diffractometer equipped with a 30 W air-cooled microfocus source (ImS) with focusing multilayer optics, with graphite-monochromated MoKα radiation (λ = 0.71073 Å). Data of **1**, **3**, **4**, **5** and **6** were collected using a Bruker-AXS D8-Venture diffractometer equipped with dual Cu/Mo source and a CMOS detector. Phi- and omega scans were used. The structures were solved using an intrinsic phasing method (ShelXT) [18]. All non-hydrogen atoms were refined anisotropically using the least-squares method on F^2 [19]. Selected crystallographic data are presented in Table 1. CCDC supplementary crystallographic data can be obtained free of charge from The Cambridge Crystallographic Data Centre via https://www.ccdc.cam.ac.uk/structures.

3. Results and discussion

3.1. Synthesis

The compounds were prepared by condensation of an acid chloride with 2-amino-4-methoxyphenol in refluxing *N*-methylpyrrolidone, according to a one-pot procedure previously used for the preparation of PBO derivatives [11]. Remarkably, the reaction mixture contained an almost equal proportion of methoxy and hydroxyl analogues, each of them obtained with a yield close to 46%, which corresponds to a very good overall condensation yield of 92%. Very likely, demethylation was catalyzed by pyridine hydrochloride formed during the reaction. According to literature, the mechanism starts with proton transfer from pyridinium ion to the aryl methyl ether, a highly unfavorable step that may account for the

Table 1. Selected crystallographic data of compounds **1** to **6**.

	1	**2**	**3**	**4**	**5**	**6**
Empirical formula	$C_{14}H_{11}NO_2$	$C_{15}H_{13}NO_2$	$C_{18}H_{19}NO_2$	$C_{13}H_9NO_2$	$C_{14}H_{11}NO_2$	$C_{17}H_{17}NO_2$
Formula weight	225.24	239.26	281.34	211.21	225.24	267.31
Crystal system	Monoclinic	Orthorhombic	Monoclinic	Monoclinic	Orthorhombic	Monoclinic
Space group	$P2_1$	$Pca2_1$	$P2_1/c$	$P2_1/n$	$P2_12_12_1$	$P2_1/c$
Unit cell dimensions						
a (Å)	11.1155(5)	12.6367(14)	9.1097(3)	5.812(3)	4.0259(2)	12.7819(4)
b (Å)	3.9025(2)	5.0487(6)	8.2557(2)	19.261(8)	10.7878(8)	8.6214(3)
c (Å)	13.2862(5)	38.014(5)	19.9688(7)	8.755(4)	25.0214(17)	13.2019(5)
β (°)	108.7336(14)	90	90.2561(15)	93.743(14)	90	104.9320(12)
Volume ($Å^3$)	545.80(4)	2425.2(5)	1501.78(8)	978.0(7)	1086.69(12)	1405.70(8)
Z	2	8	4	4	4	4
Crystal size (mm^3)	0.350 × 0.200 × 0.060	0.600 × 0.250 × 0.050	0.300 × 0.300 × 0.250	0.200 × 0.120 × 0.080	0.440 × 0.100 × 0.080	0.400 × 0.150 × 0.100
Reflections collected/independent	20789/3336 R(int) = 0.0324	23116/4938 R(int) = 0.0922	48591/3080 R(int) = 0.0919	24972/2254 R(int) = 0.0798	24504/3138 R(int) = 0.0614	57891/4117 R(int) = 0.0470
Parameters/Restraints	155/1	329/1	194/0	149/0	159/0	188/0
Final *R*1 indices I>2σ(I)	0.0383	0.0675	0.0481	0.0488	0.0479	0.0441
*wR*2 all data	0.0971	0.2053	0.1344	0.1038	0.1041	0.1257
Largest diff. peak and hole ($e.Å^{-3}$)	0.151 and -0.213	0.287 and -0.261	0.333 and -0.327	0.208 and -0.289	0.185 and -0.202	0.307 and 0.226
CCDC	1944367	1944368	1944369	1944370	1944371	1944372

high temperature required [20]. Selecting another synthesis procedure from the many that have been reported in the literature would certainly allow preparing each compound independently, with high yield. However, obtaining in one batch both compounds in significant proportions was of interest for the present work. After purification by silica chromatography, compounds **1**-**6** were characterized by usual methods (^{1}H and ^{13}C NMR, HRMS and FTIR).

3.2. Spectroscopic study in solution

All spectroscopic data are gathered in Table 2. As an example, the spectra of compounds **2** and **5** are shown in Fig. 2. The compounds were first studied in organic solutions, where they exhibited rather close properties. For every compound in *n*-heptane, as well as for the methoxy derivatives in ethanol, the absorption spectra showed two strong bands in the UV region, at 272 nm and 316 nm. For the hydroxyl derivatives in ethanol, the two bands were slightly shifted to the red and their relative intensity was reversed. The substituent in the *para* position of the phenyl group played an insignificant role. The molar extinction coefficient of **2** and **5** in ethanol was measured to be 17200 $M^{-1}.cm^{-1}$ and 14400 $M^{-1}cm^{-1}$ at the maximum of the long-wavelength band, respectively. By comparison, the spectra of compounds **7**-**9** display only one band at around 300 nm [11].

Table 2. Maximum absorption wavelength (λ_{abs}), maximum emission wavelength ($\lambda_{em.}$), fluorescence and photoluminescence quantum yields (ϕ_F and ϕ_{PL}) for compounds **1** to **6**. Dye concentration in solution around 4×10^{-5} M for absorption and 3×10^{-6} M for emission. Excitation at 310 nm for solutions and at 360 nm for the solid state. Peaks of highest intensity underlined. [a] from ref. 11.

Compound	*n*-Heptane			Ethanol			Solid state	
	$\lambda_{abs.}$	$\lambda_{em.}$	ϕ	$\lambda_{abs.}$	$\lambda_{em.}$	ϕ	$\lambda_{em.}$	ϕ
1	272, 316	360	0.50	272, 316	394	0.49	398	0.42
2	272, 316	372	0.59	272, 316	387	0.54	426	0.42
3	272, 316	360	0.57	272, 316	387	0.56	398	0.34
4	272, 312	366	0.45	274, 318	413	0.18	418	< 0.01
5	272, 314	370	0.55	274, 319	408	0.25	424	< 0.01
6	272, 314	356	0.57	276, 320	408	0.27	424	< 0.01
7 [a]	292, 298, 312	316, 330, 346	0.69	292, 298, 310	322, 336, 350	0.80	360	0.26
8 [a]	294, 302, 314	318, 334, 350	0.74	292, 302, 314	322, 338, 354	0.75	369, 383	0.34
9 [a]	294, 302, 316	318, 334, 352	0.77	292, 302, 314	324, 340, 354	0.83	362, 374	0.33

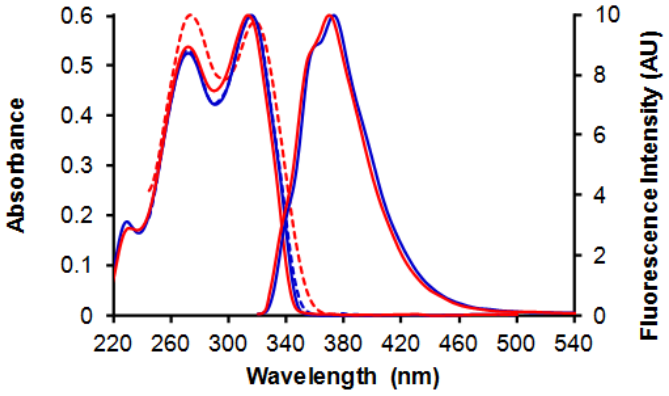

Fig. 2. Normalized UV-Vis absorption spectra (left) and fluorescence emission spectra (right) of methoxy derivative **2** (blue lines) and hydroxyl derivative **5** (red lines) dissolved in *n*-heptane (solid lines) and ethanol (dotted lines). λ_{ex} = 310 nm. Concentrations around 4×10^{-5} M for absorption and 3×10^{-6} M for emission.

All compounds were strongly fluorescent in solution. The emission spectra, recorded in dilute solutions, showed one band with weak vibrational resolution in *n*-heptane, and no resolution in ethanol. For the methoxy derivatives, the maximum was at 374 nm in *n*-heptane, slightly red-shifted in ethanol, and the quantum yield was rather high (up to 0.59) in both solvents. The hydroxyl derivatives exhibited almost the same spectra as their methoxy analogues in *n*-heptane. However, in ethanol, their emission maxima were shifted to the visible range, and their fluorescence quantum yield was reduced by half. By comparison, the parent compounds **7**-**9** emit in the UV range with a maximum around 316 nm in *n*-heptane and 322 nm in ethanol, and a high quantum yield of about 0.74 in both solvents [11].

Consequently, the substitution at position 5 by a methoxy or hydroxyl group induced the emission spectra to shift significantly to long wavelengths, and generated a solvatochromic behavior, with respect to the parent compounds. The fluorescence efficiency seems to be related to the ability of the dye molecules to form hydrogen bonds with the solvent. Due to their heteroatoms, methoxy-

substituted PBO are H-bond acceptors, and the influence of these bonds on the emission properties is quite moderate. In contrast, the hydroxyl derivatives may be involved as donors in H-bonding interactions, which may account for the strong solvatochromic behavior, and also be detrimental to the emission efficiency. Indeed, H-bond assisted nonradiative deactivation of the excited states is a well-known fluorescence quenching mechanism for various fluorophores [21]. For all our compounds in both solvents, the electron-donating effect of the methyl and *tert*-butyl group seems to increase the emission efficiency. Finally, it is noteworthy that no changes in the shape and position of the emission spectra were detected with increasing concentration up to 1.4×10^{-3} M. In particular, no excimer emission was observed in this concentration range.

3.3. Spectroscopic study in the solid state

In the solid state, the methoxy compounds emitted strong violet-blue light when illuminated by a hand-held UV lamp (365 nm), while the hydroxyl derivatives appeared dark. The emission spectra were an unresolved broad band. For **1** and **3**, the spectra were centered at the frontier between near UV and the visible range. Remarkably, the spectrum of **2** peaked in the violet range at 426 nm (Fig. 3), red-shifted by 57 nm by comparison with the reference compound **8**. The photoluminescence quantum yields (PLQY) were 0.42 for **1** and **2**, significantly increased with respect to parent compounds, and 0.34 for **3**.

For the hydroxyl derivatives, the solid-state emission spectra were in the same range of wavelength as above, but their intensity was very low, so that no accurate measurement could be performed using our apparatus. It cannot be excluded that emission arouse from traces of methoxy analogues.

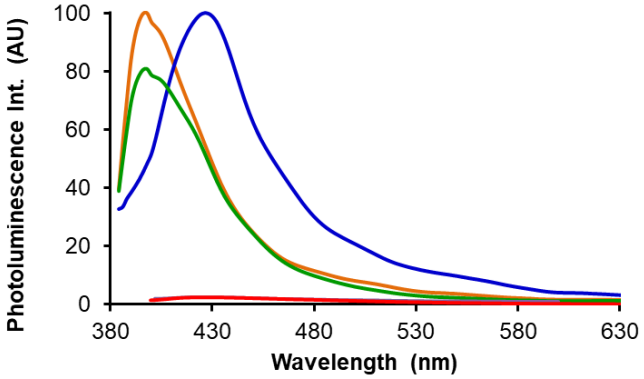

Fig. 3. Comparative solid-state emission spectra of the methoxy derivatives **1** (orange solid line), **2** (blue solid line) and **3** (green solid line), and hydroxyl derivatives **4**, **5** and **6** (red and grey lines, superimposed). The height of the spectra is proportional to the PLQY. λ_{ex} = 360 nm.

Besides, the solid-state spectroscopic properties of the 50:50 mixtures were studied. Indeed, it is now well established that solid-state fluorescence arises either from single molecules influenced by electrostatic interactions due to their bulk environment, or from excimers formed between neighboring molecules [3,4]. In both cases, energy transfer processes play an important role. This is the reason why any molecule acting as energy trap may totally quench fluorescence emission in the solid state, even at

the very low concentration of one quencher molecule per 200 [22] or 420 fluorophores [23]. Therefore, it seemed instructive to know whether or not the fluorescence of the methoxy derivatives is quenched by the presence of some hydroxyl derivative. To this aim, solid samples containing an equal proportion of methoxy and hydroxyl analogues were prepared by mixing dichloromethane solutions of the pure compounds, followed by slow evaporation of the solvent. All the samples were fluorescent under UV illumination. The position of the emission spectra was almost unchanged and the quantum yields were approximately reduced by five with respect to pure methoxy compounds.

3.4. Crystallographic study

Single crystals were grown by slow evaporation of organic solutions of the six compounds. The results of the X-ray analysis are illustrated in Fig. 4 to 6. Regarding molecular geometry, a deviation from planarity was observed with passing from methoxy to hydroxyl derivatives, and with increasing the bulkiness of the R^2 substituent. For instance, the dihedral angle between the benzoxazole heterocycle and the phenyl ring was below 1° for **1** and reached 27 ° for compound **6** (Fig. 4). Most likely, the driving force in packing was to maximize the number and strength of interactions, and packing has taken place here at the expense of planarity. This result is noticeable because the PBO framework is generally planar, whatever the substituent in the *para* position of the phenyl group [11, 24-28].

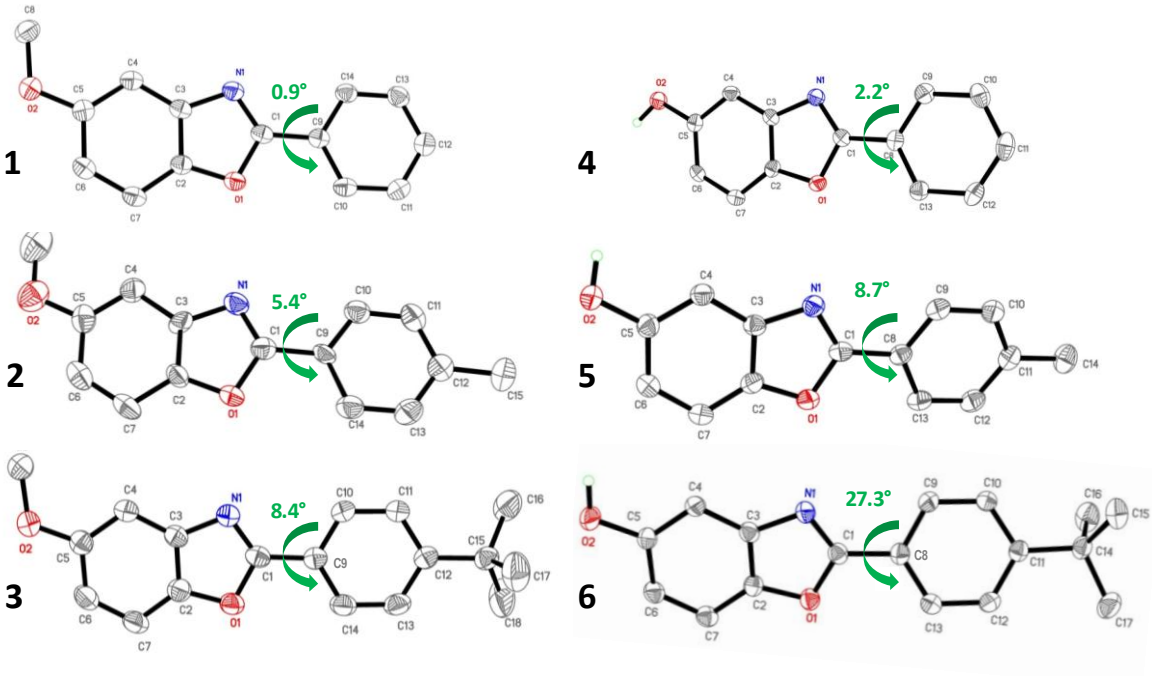

Fig. 4. Molecular views of compounds **1** to **6**.

The molecular arrangement was also closely linked to the nature of the R^1 and R^2 substituents. With regards to the methoxy derivatives (Fig. 5), for compound **1**, a molecule and the one situated immediately above point in the same direction and are laterally shifted, so that their aromatic systems

weakly overlapped. These dimers then adopt a herringbone pattern. For compound **2**, superimposed molecules also face the same direction, but they are longitudinally shifted one with respect to the other, with significant overlap of their aromatic systems. Besides, the molecules displayed crossed arrangement, as already reported for many PBO derivatives [11, 24-28]. For compound **3**, the steric hindrance due to the *tert*-butyl group induces the stacked molecules to form anti-parallel dimers, with very little overlap. The dimers then display a herringbone arrangement. For the three methoxy compounds, the plane-to-plane intermolecular distance was slightly increased with increasing the bulkiness of the substituent in the *para*-position of the phenyl group (i.e. 3.46 Å and 3.58 Å for **1** and **3**, respectively).

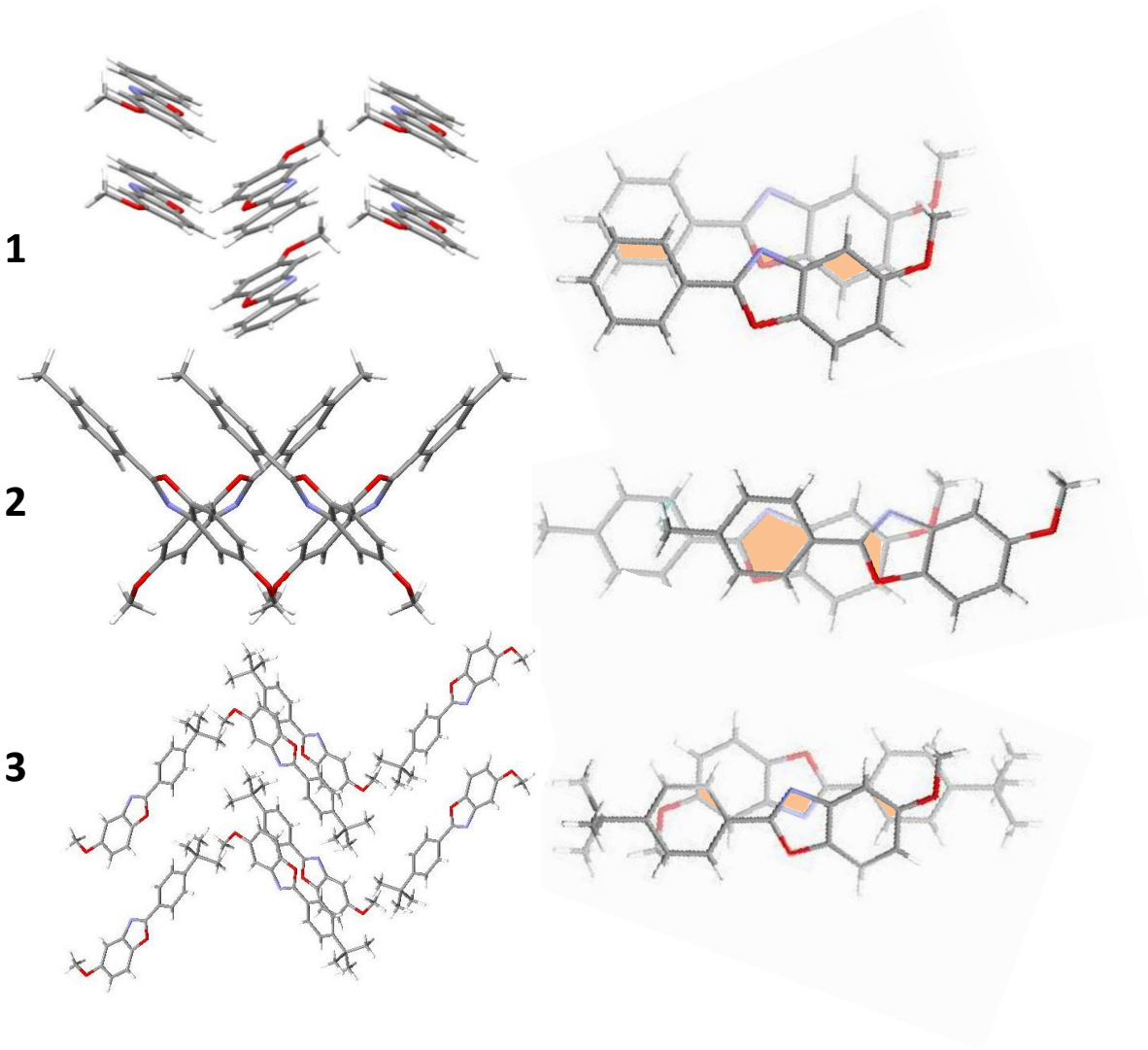

Fig. 5. Left column: Crystal packing of the methoxy derivatives **1**, **2** (view along a) and **3** (view along a). Right column: overlap of the aromatic moieties.

Considering now the three hydroxyl derivatives, the striking feature is that their organization is totally structured by hydrogen bonds (Fig. 5) [29]. More precisely, H-bonds take place between the nitrogen atom of one molecule and the hydroxyl group of the closest molecule situated in another plane, resulting in a closely intertwined molecular network. For compound **4**, molecules are situated in two different planes, and stacked molecules are displayed antiparallel. For compound **5**, molecules occupy

four different planes (not represented), which are connected by pairs owing to H-bonds. Stacked molecules are displayed parallel. For compound **6**, the molecules displayed on two different planes formed crossed arrangement. In the three cases, the aromatic systems of stacked molecules have little overlap due to lateral and/or longitudinal shift of molecules with respect to each other. The spacing between stacked molecules was increased from 3.42 Å for **4** to 4.04 Å for **6**, showing the value of the bulky *ter*-butyl group to separate the molecules in the crystal.

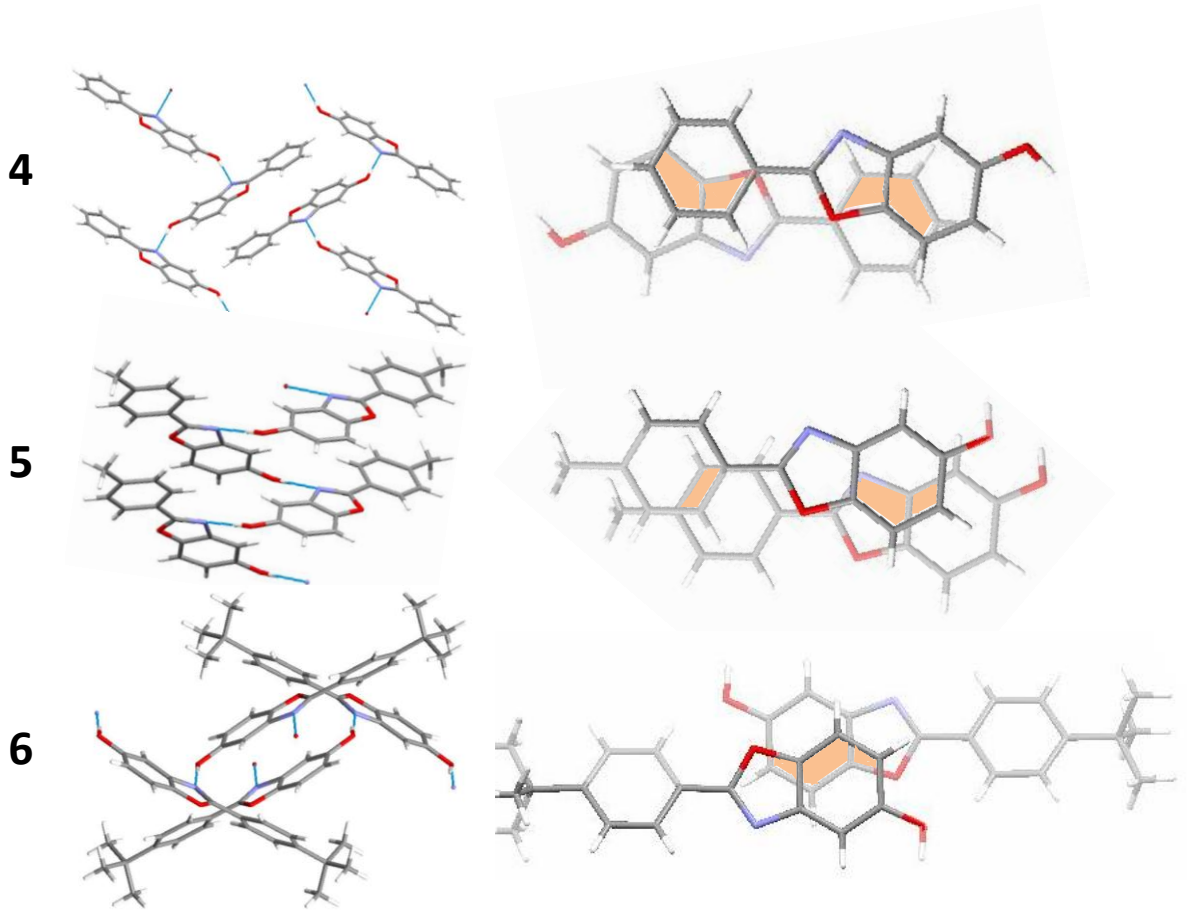

Fig. 6. Left column: Crystal packing of the hydroxyl derivatives **4** (view along a), **5** and **6** (view along c). Right column: overlap of the aromatic moieties. Hydrogen bonds are in blue ink.

In summary, the molecular arrangement is different for each compound, but in every case it should be favorable to light emission because π-stacking interactions are quite small, as is the case for most of the members of the PBO family investigated to date. Remarkably, among the three compounds that emit in the solid state, compound **2** exhibits the largest overlap of aromatic moieties. This could explain the strong red-shift of its emission spectrum compared to compounds **1** and **3**. From a molecular viewpoint, emission in organic crystals is often assumed to arise from high-energy excimers, but it may also come from single fluorophores influenced by their bulk surrounding environment [30]. Calculations could allow us to distinguish between both mechanisms. As expected, the bulky *tert*-butyl group separates the molecules. However, these positive trends are counterbalanced by the deviation of the molecular planarity, and this may explain why the introduction of the bulky *tert*-butyl group did not lead to superior fluorescence properties. Moreover, strong H-bonds take place in hydroxyl derivatives, and are probably responsible for the very weak fluorescence of these compounds in the solid state. The

effect is spectacular because the groups involved in H-bonds are directly borne by the electron conjugated system, and not only used to control the distance between and the relative orientation of electronically independent fluorophores [31].

3.5. Crystal habits

For use as materials, the homogeneity and crystallinity of the active layer are often very important. Therefore, the solids obtained after drop casting and air drying of dichloromethane solutions (1×10^{-2} M) were examined. Both techniques gave the same type of crystals, with the difference that the crystals obtained by drop casting were much smaller and often arranged around a nucleation center. Most of the compounds gave platelets. An example is given for **2** in Fig. 7a. Generally speaking, the hydroxyl derivatives gave crystals with a more defined shape. For instance, **4** provided diamond-shaped platelets, and **5** led to beautiful needles of very regular gauge (Fig. 7b), a tendency already reported for methyl-PBO [11]. Interestingly, a 50:50 mixture of **2** and **5** resulted in rods terminated by microfibers, possibly due to the fact that the less soluble compound, which crystallizes first, was used as a template by the second one (Fig. 7c). In contrast, the mixture of **3** and **6** was amorphous.

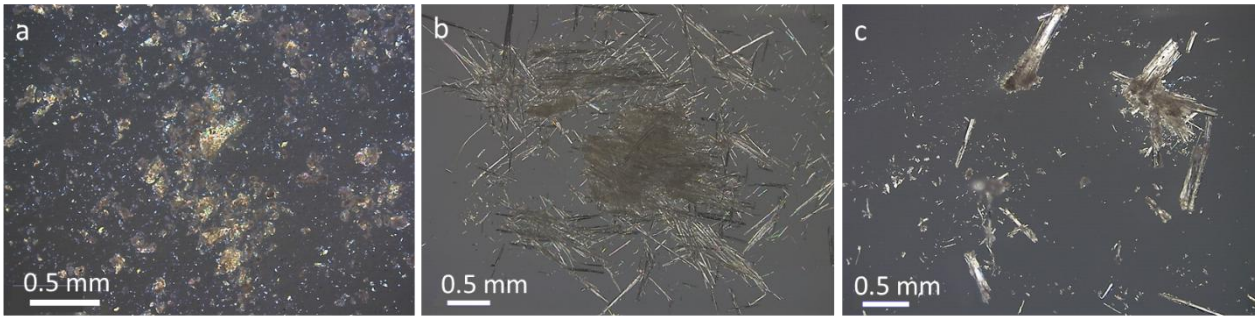

Fig. 7. Observation by polarized microscopy of the crystals formed after slow evaporation of dichloromethane solutions of compounds **2** (a), **5** (b) and an equimolecular mixture of **2** and **5** (c).

4. Conclusion

This work showed that the substitution pattern of our PBO derivatives strongly influence their fluorescence properties. The presence of a weak electron donor group at position 5 is enough to shift the emission spectra to the red with respect to parent compounds. The key factor for optical properties is indeed the capacity of this substituent to be involved in H-bonds. For instance, the methoxy derivatives could be used as fluorescent tracers in solvents of various polarities and are efficient light emitters in the solid state. In contrast, the hydroxyl derivatives have attractive properties in a nonpolar medium, but lose their appeal in polar solvents due to detrimental H-bonds with solvent molecules. In the solid state, intermolecular H-bonds become preponderant and result in almost total quenching of photoluminescence. Remarkably, the role of the bulky *tert*-butyl group is more complex than expected. Combining a methoxy group at position 5 with a methyl group at the *para* position of the phenyl ring, the best solid-state emitter, i.e. compound **2**, was obtained.

The dye mixtures, directly obtained from synthesis with very low production costs, keep moderate photoluminescence efficiency. The elongated shape of the crystals obtained in mixtures of **2**

and **5** is an advantage for applications such as the authentication of precious documents, while the amorphousness of other mixtures could be appreciated for applications in optoelectronics. By selecting the proper substitution pattern, these cheap molecules could be adapted to suit a variety of applications in the field of photoluminescent materials.

Acknowledgements

ANR is gratefully acknowledged for funding (SUPERFON project # ANR-17-CE07-0029-03).

References

[1] J.-H. Lee, C.-H. Chen, P.-H. Lee, H.-Y. Lin, M.-K. Leung, T.-L. Chiu, C.-F. Lin, Blue organic light-emitting diodes: current status, challenges, and future outlook. J. Mater. Chem. C 7 (2019) 5874–5888. DOI: 10.1039/c9tc00204a

[2] Y. Im, S.Y. Byun, J.H. Kim, D.R. Lee, C.S. Oh, K.S. Yook, J.Y. Lee, Recent progress in high-efficiency blue-light-emitting materials for organic light-emitting diodes. Adv. Funct. Mater. 27 (2017) 1603007. DOI: 10.1002/adfm.201603007

[3] J. Cornil, D. Beljonne, D.A. Dos Santos, J.P. Calbert, Z. Shuai, J. L. Brédas, A theoretical insight into the solid-state optical properties of luminescent materials: the supermolecular approach. C. R. Acad. Sci. Paris Series IV (2000) 403−408.

[4] L. Wilbraham, C. Adamo, F. Labat, I. Ciofini, Electrostatic embedding to model the impact of environment on photophysical properties of molecular crystals: A self-consistent charge adjustment procedure. J. Chem. Theory Comput. 12 (2016) 3316−3324 and ref. cited.
DOI: 10.1021/acs.jctc.6b00263

[5] S.P. Anthony, Organic solid-state fluorescence: Strategies for generating switchable and tunable fluorescent materials. ChemPlusChem 77 (2012) 518−531. DOI: 10.1002/cplu.201200073

[6] C. Carayon, S. Fery-Forgues, 2-Phenylbenzoxazole derivatives: a family of robust emitters of solid-state fluorescence. Photochem. Photobiol. Sci. 16 (2017) 1020−1035. DOI: 10.1039/c7pp00112f

[7] H. Jo, K. Kim, D. E. Kim, H. K. Shin, B. J. Lee, Synthesis of phosphine oxides with tris(benzoxazole/benzothiazole) moieties and their OLED characteristics. Mol. Cryst. Liq. Cryst. 6 (2016) 60−66. DOI: 10.1080/15421406.2016.1200944

[8] C.-W. Ko, Y.-T. Tao, A. Danel, L. Krzeminska, P. Tomasik, Organic light-emitting diodes based on 2-(stilben-4-yl)benzoxazole derivatives: An implication on the emission mechanism. Chem. Mater. 13 (2001) 2441−2446. DOI: 10.1021/cm010199u

[9] N. Abid-Jarraya, H. Turki-Guermazi, K. Khemakhem, S. Abid, N. Saffon, S. Fery-Forgues, Investigations in the methoxy-iminocoumarin series: Highly efficient photoluminescent dyes and easy preparation of green-emitting crystalline microfibers. Dye Pigm. 101 (2014) 164−171. DOI: 10.1016/j.dyepig.2013.09.043

[10] K. Khemakhem, M. Soulié, R. Brousses, H. Ammar, S. Abid, S. Fery-Forgues, Small iminocoumarin derivatives as red emitters: From biological imaging to highly photoluminescent non-doped micro- and nanofibers. Chem. Eur. J. 21 (2015) 7927–7937. DOI: 10.1002/chem.201406563

[11] A. Ghodbane, S. D'Altério, N. Saffon, N.D. McClenaghan, L. Scarpantonio, P. Jolinat, S. Fery-Forgues, Facile access to highly fluorescent nanofibers and microcrystals via reprecipitation of 2-phenyl-benzoxazole derivatives. Langmuir 28 (2012) 855–863. DOI:10.1021/la2036554

[12] Z. Li, G. Gan, Z. Ling, K. Guo, C. Si, X. Lv, H. Wang, B. Wei, Y. Hao, Easily available, low-cost 9,9'-bianthracene derivatives as efficient blue hosts and deep-blue emitters in OLEDs. Org. Electron. 66 (2019) 24–31. DOI: 10.1016/j.orgel.2018.12.010

[13] Y. Wang, D. Xu, H. Gao, Y. Wang, X. Liu, A. Han, C. Zhang, L. Zang, Twisted donor-acceptor cruciform luminophores possessing substituent-dependent properties of aggregation-induced emission and mechanofluorochromism. J. Phys. Chem. C 122 (2018) 2297−2306. DOI: 10.1021/acs.jpcc.7b11368

[14] M.-M. Shi, V.C. Tung, J.-J. Nie, H.-Z. Chen, Y. Yang, Bulky rigid substitutions: A route to high electron mobility and high solid-state luminescence efficiency of perylene diimide. Org. Electron. 15 (2014) 281–285. DOI: 10.1016/j.orgel.2013.11.011
[15] J.-Y. Hu, M. Era, M.R.J. Elsegood, T. Yamato. Synthesis and photophysical properties of pyrene-based light-emitting monomers: Highly pure-blue-fluorescent, cruciform-shaped architectures. Eur. J. Org. Chem. (2010) 72–79. DOI: 10.1002/ejoc.200900806
[16] C. Würth, M. Grabolle, J. Pauli, M. Spieles, U. Resch-Genger, Relative and absolute determination of fluorescence quantum yields of transparent samples. Nature Prot. 8 (2013) 1535–1550. DOI: 10.1038/nprot.2013.087
[17] J.C. De Mello, H.F. Wittmann, R.H. Friend, An improved experimental determination
of external photoluminescence quantum efficiency, Adv. Mater. 9 (1997) 230–232. DOI : 10.1002/adma.19970090308
[18] G.M. Sheldrick, SHELXT – Integrated space-group and crystal structure determination. Acta Cryst. A 71 (2015) 3–8. DOI:10.1107/S2053273314026370
[19] G.M. Sheldrick, Crystal structure refinement with SHELXL. Acta Cryst. C 71 (2015) 3–8. DOI: 10.1107/S2053229614024218
[20] R.L. Burwell, The Cleavage of Ethers. Chem. Rev. 54 (1954) 615–685. DOI:10.1021/cr60170a003
[21] S.F. Lee, Q. Vérolet, A. Fürstenberg, Improved super-resolution microscopy with oxazine fluorophores in heavy water. Angew. Chem. Int. Ed. 52 (2013) 8948–8951, and ref. herein. DOI: 10.1002/anie.201302341
[22] I. Shulov, S. Oncul, A. Reisch, Y. Arntz, Ma. Collot, Y. Mely, A.S. Klymchenko, Fluorinated counterion-enhanced emission of rhodamine aggregates: ultrabright nanoparticles for bioimaging and light-harvesting. Nanoscale, 7 (2015) 18198–18210. DOI: 10.1039/c5nr04955e
[23] J. Su, T. Fukaminato, J.-P. Placial, T. Onodera, R. Suzuki, H. Oikawa, A. Brosseau, F. Brisset, R. Pansu, K. Nakatani, R. Métivier, Giant amplification of photoswitching by a few photons in fluorescent photochromic organic nanoparticles. Angew. Chem. Int. Ed. 55 (2016) 3662–3666. DOI: 10.1002/anie.201510600
[24] A. Ghodbane, P. Bordat, N. Saffon, S. Blanc, S. Fery-Forgues, From 2-phenylbenzoxazole to diphenyl-bibenzoxazole derivatives: Comparative advantages of mono- and bis-chromophores for solution and solid-state fluorescence. Dye Pigm. 125 (2016) 282–291. DOI: 10.1016/j.dyepig.2015.10.027
[25] A. Ghodbane, N. Saffon, S. Blanc and S. Fery-Forgues, Influence of the halogen atom on the solid state fluorescence properties of 2-phenyl-benzoxazole derivatives, Dye. Pigm. 113 (2015) 219–226. DOI:10.1016/j.dyepig.2014.08.011
[26] A. Ghodbane, W. B. Fellows, J. Bright, D. Ghosh, N. Saffon, L. M. Tolbert, S. Fery-Forgues and K. M. Solntsev, Effects of the benzoxazole group on green fluorescent protein chromophore crystal structure and solid state photophysics. J. Mater. Chem. C 14 (2016) 2793–2801. DOI: 10.1039/c5tc03776j
[27] Y. Qian, M. Cai, X. Zhou, Z. Gao, X. Wang, Y. Zhao, X. Yan, W. Wei, L. Xie and W. Huang, More than restriction of twisted intramolecular charge transfer: Three-dimensional expanded #-shaped cross-molecular packing for emission enhancement in aggregates, J. Phys. Chem. C 116 (2012) 12187−12195. DOI: 10.1021/jp212257f
[28] L. Wang, Y. Shen, M. Yang, X. Zhang, W. Xu, Q. Zhu, J. Wu, Y. Tian and H. Zhou, Novel highly emissive H-aggregates with aggregate fluorescence change in a phenylbenzoxazole-based system. Chem. Commun. 50 (2014) 8723-8726. DOI: 10.1039/c4cc02564d
[29] A. Ramanan, G.R. Desiraju, J.J. Vittal, Crystal Engineering: A Textbook. Cambridge University Press/World Scientific (2011). ISBN 10: 9814366862, ISBN 13: 9789814366861.
[30] D. Presti, L. Wilbraham, C. Targa, F. Labat, A. Pedone, M.C. Menziani, I. Ciofini, C. Adamo. J. Phys. Chem. C 121 (2017) 5747–5752. DOI: 10.1021/acs.jpcc.7b00488
[31] A.T. Haedler, H. Misslitz, C. Buehlmeyer, R.Q. Albuquerque, A. Kçhler, H.-W. Schmidt, Controlling the π-stacking behavior of pyrene derivatives: Influence of H-bonding and steric effects in different states of aggregation. ChemPhysChem 14 (2013) 1818–1829. DOI: 10.1002/cphc.201300242